A Ball-in-Bowl Wave Energy Harvester

Oliver Chang[a], Reza Alam[a,1,*]

[a]*Department of Mechanical Engineering, University of California, Berkeley, CA, 94563*

Abstract

Write a concise abstract here (typically 150 - 250 words).

Keywords: Ocean engineering, Wave modelling, Hydrodynamics, Offshore structures

1. Introduction

Autonomous surface vessels (ASVs) have emerged as critical platforms for oceanographic research, environmental monitoring, and maritime surveillance. While these platforms offer reduced operational costs and extended mission capability, their fundamental limitation remains energy supply. Traditional battery-powered systems require periodic return to port, while fuel-based systems add weight and environmental concerns. For applications requiring persistent ocean presence, modern low-power sensors and communication systems typically demand 1 - 50 W continuous power, yet even this modest requirement can exhaust onboard batteries within days [1, 2]. This constraint has motivated extensive research into harvesting renewable energy from the marine environment.

The unmanned surface vehicle considered in this work employs a hybrid power generation system harvesting energy from three complementary modalities: solar, wind, and wave. Solar photovoltaic panels provide the highest peak power output but suffer from intermittency due to day - night cycles and cloud coverage. Wind energy harvesting generates lower peak power compared to solar but offers greater consistency, continuing to operate during overcast conditions and nighttime. Wave energy serves as a critical third modality: when both solar and wind become unavailable - such

*Corresponding author.
Email address: reza.alam@berkeley.edu (Reza Alam)

as during calm, overcast nights - ocean waves typically persist, providing a continuous source of power. Wave harvesters can operate up to 90% of the time compared to 20 - 40% for solar and wind systems [3, 4]. The expectation for wave energy harvesting is not to generate large amounts of power, but rather to serve as a small yet reliable and continuous source that complements the other two modalities, significantly increasing overall system reliability.

Given the space and mass constraints inherent to small autonomous vessels, the wave energy harvester must be compact and lightweight. Since the vessel is expected to operate autonomously for extended periods, system reliability is paramount. These requirements favor designs with minimal moving parts housed within a fully enclosed container, eliminating components in direct contact with seawater. Such encapsulation protects against salt spray, biofouling, and corrosion - the primary failure mechanisms for marine equipment [1]. Electromagnetic harvesters employing a magnet sliding or rolling inside a coil-wound enclosure satisfy these criteria, as the entire mechanism can be sealed within a waterproof housing with no external moving parts.

Electromagnetic vibration energy harvesters operate on Faraday's law, where relative motion between a permanent magnet and a conductive coil induces an electromotive force proportional to the rate of flux change: $e = -N\,\mathrm{d}\Phi/\mathrm{d}t$. The canonical framework for vibration energy harvesting establishes characteristic equations comparing electromagnetic, piezoelectric, and electrostatic transduction mechanisms [5]. Among these, electromagnetic transduction is most suitable for ocean vehicles requiring watt-level power output, as piezoelectric and triboelectric harvesters typically generate only microwatts to tens of milliwatts [6, 7]. A "springless proof-mass" architecture, where the magnet moves freely without mechanical springs, suits the low-frequency, irregular excitations characteristic of ocean waves. When the magnet follows a curved path, the system exhibits nonlinear restoring forces modeled using the Duffing equation [8], with nonlinear response improving energy harvesting through broadband frequency response.

Compared to mechanical machinery-based vibration sources, ocean wave-induced motions are particularly challenging for energy harvesting because of their low-frequency content (typically 0.1 - 1 Hz), large amplitudes, aperiodic nature, and generally unpredictable and time-varying signatures [9]. Traditional high-Q resonant harvesters are tuned for maximum power output over a narrow frequency range, rendering them ineffective for the broadband spectral content of irregular ocean waves. Furthermore, achieving resonant frequencies below 1 Hz in compact devices requires impractically compliant

spring elements and large displacement allowances [9]. These limitations motivate non-resonant architectures that can produce useful output power across a wide range of excitation amplitudes, directions, and frequencies.

Inertial pendulum-based harvesters have received considerable attention for low-frequency ocean applications due to their inherent low-frequency characteristics and adaptability to irregular excitations [10–12]. According to swing axis arrangement, pendulum mechanisms can be categorized into horizontal-axis, vertical-axis, inclined-axis, and gimbaled types [13]. Horizontal-axis designs have achieved 0.13 - 0.72 W output but cannot effectively capture wave vibration from random directions [14–16]. Gimbaled pendulum mechanisms capable of multi-DOF swinging offer superior multi-directional adaptability with compact structure [13, 17]. A hemispherical biaxial-pendulum harvester achieved 2.03 W peak power and 256 $\mathrm{W/m^3}$ power density at 1.5 - 2.2 Hz [10], while an optimized spherical multi-DOF design demonstrated 25.45% energy conversion efficiency at 1.0 Hz with sea trials confirming operation across the 0.2 - 1.0 Hz range typical of ocean conditions [13].

Rolling magnet configurations offer distinct advantages over sliding designs for enclosed electromagnetic harvesters. Rolling action inherently dissipates less energy than sliding due to reduced friction losses [9, 18], making it preferable for low-power marine applications where every milliwatt matters. Non-resonant rolling designs also exhibit frequency up-conversion behavior, where low-frequency mechanical input (approximately 1 - 15 Hz) is transformed into higher-frequency electrical output (approximately 5 - 25 Hz) through the free mechanical motion of the rolling element [9]. Parametric studies have shown that the optimal ball-to-cavity diameter ratio depends on excitation amplitude: smaller ratios suit lower-amplitude excitations by allowing the ball to be excited into large motions, while larger ratios are preferable for higher-amplitude inputs that can easily move a larger mass [9]. Radially magnetized rolling cylinders have generated milliwatt-scale power, with controlled friction effects reported to increase output [19].

Track geometry and magnetic potential configuration significantly influence harvester performance. The cycloid curve has been reported to improve performance relative to straight and circular geometries [20], while Halbach arrays can improve electromagnetic coupling [21]. Multi-well magnetic potential configurations enable broadband operation through snap-through transitions across potential wells [22]. Two-well and three-well systems can exhibit chaotic zones that cause irregular power generation [23]. Hybrid wind -

wave harvesters for unmanned surface vessels have been demonstrated [24], and commercial wave-powered platforms have logged multi-year deployments and multi-million nautical-mile endurance [25]. However, cyclic mechanical loading between rolling surfaces can cause progressive coating degradation, reinforcing the importance of materials selection for long-duration marine deployment [23].

This paper investigates electromagnetic energy harvesting from ocean wave-induced motion as the third modality in a hybrid power system for autonomous surface vessels. We analyze a configuration employing a permanent magnet rolling over a coil-covered curved surface within a sealed enclosure, optimized for ultra-low-frequency ocean waves. The objectives are to derive governing equations with electromagnetic damping, optimize track geometry for maximum power extraction, and evaluate feasibility for providing continuous supplementary power for marine electronics.

2. Dynamics and Energy Harvesting Analysis of a Ball Rolling Inside a Pendulum-Mounted Spherical Bowl

2.1. Problem formulation

Consider a spherical bowl of inner radius R_i rigidly attached to a pendulum that swings about a fixed pivot point, as illustrated in Figure 1. A solid sphere (ball) of mass m and radius r rolls without slipping on the inner surface of the bowl. The pendulum swing is prescribed as $\alpha(t) = \alpha_0 \sin(\Omega t)$, representing external excitation from an environmental source such as ocean waves. The objective is to derive the equation of motion governing the ball dynamics and analyze the system's potential for energy harvesting.

The coordinate system is established with the origin at the fixed pivot point, with X directed horizontally to the right and Y directed vertically upward. Rotations follow the standard mathematical convention where counterclockwise (CCW) is positive. The pendulum angle $\alpha(t)$ is measured counterclockwise from the downward vertical, such that $\alpha > 0$ corresponds to the bowl swinging to the right ($+X$ direction). The ball position angle $\beta(t)$ is measured counterclockwise from the bowl's tilted symmetry axis, with $\beta > 0$ indicating rightward displacement relative to the bowl centerline. The total angle of the ball from the laboratory vertical is thus $\theta = \alpha + \beta$. The key geometric parameters include the effective pendulum length $\ell = d - R_i$, where d is the distance from the pivot to the lowest point of the bowl's inner surface,

and the effective radius $R = R_i - r$, representing the distance from the bowl center to the ball center.

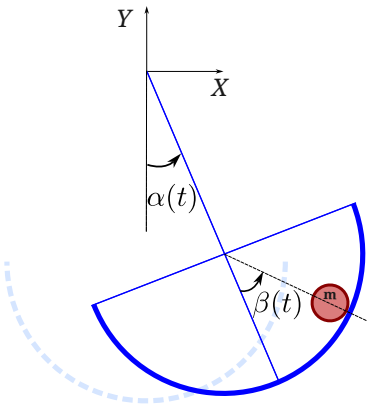

Figure 1: Schematic of the ball-in-bowl wave energy harvester showing the two degrees of freedom. The bowl (dark blue arc) pivots about the origin of the inertial XY frame by angle $\alpha(t)$ driven by wave-induced platform motion. The ball of mass m rolls along the concave surface at angle $\beta(t)$ measured from the bowl centerline.

2.2. Derivation of the governing equation

The equations of motion are derived using Lagrangian mechanics. Using the convention that a unit vector at angle ϕ measured counterclockwise from the downward vertical is $(\sin\phi, -\cos\phi)$, the position of the ball center in the laboratory frame is

$$X_b = \ell \sin\alpha + R\sin(\alpha+\beta), \qquad Y_b = -\ell\cos\alpha - R\cos(\alpha+\beta). \tag{1}$$

These expressions place the ball at $(0, -\ell - R)$ when $\alpha = \beta = 0$, and yield $X_b > 0$ for small positive angles.

The rolling constraint (zero relative velocity at the contact point between the ball and bowl surfaces) yields the ball angular velocity

$$\omega_b = \dot{\alpha} - \frac{R}{r}\dot{\beta}. \tag{2}$$

When the ball moves CCW along the bowl (increasing β), it must spin clockwise relative to the bowl to maintain rolling contact.

The total kinetic energy comprises translational and rotational components. The translational kinetic energy is $T_{\text{trans}} = \frac{1}{2}mv_b^2$, where

$$v_b^2 = \ell^2\dot{\alpha}^2 + R^2(\dot{\alpha}+\dot{\beta})^2 + 2\ell R\dot{\alpha}(\dot{\alpha}+\dot{\beta})\cos\beta. \tag{3}$$

The rotational kinetic energy is $T_{\text{rot}} = \frac{1}{2}I\omega_b^2$ with the solid-sphere moment of inertia $I = \frac{2}{5}mr^2$, i.e.

$$T_{\text{rot}} = \frac{1}{5}m\big(r\dot{\alpha} - R\dot{\beta}\big)^2. \tag{4}$$

The potential energy, referenced to the pivot location, is

$$U = -mg\big(\ell\cos\alpha + R\cos\theta\big). \tag{5}$$

Applying the Euler - Lagrange equation with β as the generalized coordinate yields the nonlinear equation of motion. Including viscous damping with internal coefficient c_i (mechanical losses) and load coefficient c_L (energy extraction), the governing equation is

$$\frac{7}{5}R\,\ddot{\beta} + \frac{(c_i+c_L)R}{m}\dot{\beta} + \left(R - \frac{2r}{5} + \ell\cos\beta\right)\ddot{\alpha} + \ell\sin\beta\,\dot{\alpha}^2 + g\sin(\alpha+\beta) = 0. \tag{6}$$

The term proportional to $\ddot{\alpha}$ couples the prescribed bowl motion to the ball response, while $\ell\sin\beta\,\dot{\alpha}^2$ represents a centrifugal effect due to the pendulum's circular motion.

2.3. Linearized dynamics and natural frequency

For small angular displacements where $|\alpha|, |\beta| \ll 1$, we use $\sin(\alpha+\beta) \approx \alpha+\beta$, $\cos\beta \approx 1$, and $\sin\beta \approx \beta$. The parametric term $\ell\beta\dot{\alpha}^2$ is second-order small and is neglected. The linearized equation becomes

$$\frac{7}{5}R\,\ddot{\beta} + \frac{(c_i+c_L)R}{m}\dot{\beta} + g\beta = -g\alpha - \kappa\ddot{\alpha}, \tag{7}$$

where the coupling parameter is

$$\kappa = \ell + R - \frac{2r}{5} = d - \frac{7r}{5}. \tag{8}$$

For harmonic excitation $\alpha(t) = \alpha_0\sin(\Omega t)$, Eq. (7) can be written as a forced harmonic oscillator,

$$\ddot{\beta} + 2\zeta_T\omega_n\dot{\beta} + \omega_n^2\beta = F_0\sin(\Omega t), \tag{9}$$

where $\zeta_T = \zeta_i + \zeta_L$ is the total damping ratio, with ζ defined through $\zeta = 5c/(14m\omega_n)$. The natural frequency is

$$\omega_n = \sqrt{\frac{5g}{7R}} = \sqrt{\frac{5g}{7(R_i - r)}}. \tag{10}$$

The forcing amplitude is $F_0 = -\alpha_0\omega_n^2\big(1 - \kappa\Omega^2/g\big)$, which at resonance ($\Omega = \omega_n$) gives

$$|F_0| = \alpha_0\omega_n^2\left|1 - \frac{5\kappa}{7R}\right|. \tag{11}$$

The factor $\left(1 - \frac{5\kappa}{7R}\right)$ reveals a null condition: when $\kappa = \frac{7R}{5}$ (equivalently $d/R_i = 1.4$), gravitational forcing from the tilted bowl and inertial forcing from the bowl acceleration cancel, resulting in minimal ball response. This null should be avoided in practical designs (e.g., by selecting $d/R_i < 1.2$ or $d/R_i > 1.6$).

2.4. Power extraction and optimal design

The time-averaged power extracted by the load damping mechanism at resonance is

$$\bar{P}_L = \frac{7mR^2F_0^2}{20\omega_n}\,\frac{\zeta_L}{(\zeta_i + \zeta_L)^2}. \tag{12}$$

Maximizing (12) with respect to ζ_L yields the impedance-matching condition $\zeta_L = \zeta_i$, at which

$$\bar{P}_{L,\max} = \frac{7mR^2F_0^2}{80\zeta_i\omega_n}. \tag{13}$$

Under this optimal condition, the harvesting efficiency (extracted power divided by total dissipated power) is 50%, with the remaining power lost to internal mechanical dissipation. The corresponding steady-state amplitude is

$$\beta_0 = \frac{|F_0|}{4\zeta_i\omega_n^2}. \tag{14}$$

2.5. Design procedure

The design procedure is summarized in the flowchart of Figure 2. Given the excitation period T and amplitude α_0, along with an estimate of internal damping ζ_i, the designer first selects the ball geometry (radius r and mass m) based on practical constraints, and chooses the pivot distance d to avoid

the null point at $d/R_i = 1.4$. The effective radius for resonance is then calculated as $R = 5g/(7\Omega^2)$ (with $\Omega = 2\pi/T$), from which the required bowl inner radius follows as $R_i = R + r$. The coupling parameter $\kappa = d - \frac{7r}{5}$ and forcing amplitude are subsequently evaluated.

If the predicted optimal amplitude $\beta_{0,\text{opt}} = |F_0|/(4\zeta_i\omega_n^2)$ falls within acceptable geometric limits (typically $\beta_{\max} < 45^\circ$ to maintain validity of the small-angle approximation and ensure continuous contact), the system operates under impedance-matched conditions with $\zeta_L = \zeta_i$ and 50% efficiency. Otherwise, the design becomes amplitude-limited, requiring increased load damping

$$\zeta_L = \frac{|F_0|}{2\omega_n^2\beta_{\max}} - \zeta_i \tag{15}$$

to constrain the motion, resulting in higher efficiency but reduced absolute power output. A final validity check ensures $\zeta_L > 0$ and confirms that the small-angle assumptions remain appropriate for the predicted operating conditions.

3. Design Considerations

3.1. Bowl material selection

The selection of the bowl material is governed by three primary constraints: magnetic neutrality, minimal frictional losses, and suppression of eddy-current dissipation. The bowl must be fabricated from a non-ferromagnetic material to avoid distorting the magnetic field of the rolling sphere, which would otherwise reduce the flux linkage with the pickup coils. Simultaneously, the material must exhibit a low coefficient of rolling friction to preserve the kinetic energy of the sphere; typical rolling-friction coefficients range from 0.01 to 0.05 for hard polymer-on-metal contacts, compared to 0.2 to 0.5 for sliding interfaces.

Perhaps most critically, the material must be electrically non-conductive (or sufficiently thin) to minimize eddy-current losses, which scale with the product of electrical conductivity σ and wall thickness t according to

$$P_{\text{eddy}} \propto \sigma\, t \left(\frac{\mathrm{d}\Phi}{\mathrm{d}t}\right)^2, \tag{16}$$

where Φ denotes the magnetic flux through the conductive wall. Conductive materials such as aluminum, despite their excellent machinability, can dis-

sipate a significant fraction of the harvested energy as heat unless the bowl wall thickness is reduced below approximately 0.5 mm.

Several candidate materials satisfy these requirements to varying degrees. Polytetrafluoroethylene (PTFE) offers an exceptionally low friction coefficient (approximately 0.04) and complete electrical insulation, though its relatively low hardness may lead to surface wear over extended operation. Polyether ether ketone (PEEK) provides superior mechanical strength and wear resistance with comparable electrical properties, albeit at substantially higher cost. Acrylic and additively manufactured thermoplastics such as PLA or PETG represent cost-effective alternatives suitable for prototyping, with friction coefficients in the range 0.04 to 0.08 depending on surface finish. For applications requiring precise curvature and smooth surface topology, CNC-machined PTFE or injection-molded PEEK appear to be the most promising candidates, balancing tribological performance against manufacturing feasibility and long-term durability.

4. Methods

Describe the methodology, data, and experimental or numerical setup.

5. Results

Present results with appropriate figures and tables.

6. Discussion

Interpret results and relate to prior work.

7. Conclusions

Summarize the main findings and outline future work.

Acknowledgements

(Optional) Acknowledge funding and contributions.

References

[1] J. Graves, Y. Kuang, M. Zhu, Counterweight-pendulum energy harvester with reduced resonance frequency for unmanned surface vehicles, Sensors and Actuators A: Physical 321 (2021) 112577.

[2] A. Mendez, T. J. Leo, M. A. Herreros, Current state of technology of fuel cell power systems for autonomous underwater vehicles, Energies 7 (7) (2014) 4676–4693.

[3] B. Drew, A. R. Plummer, M. N. Sahinkaya, A review of wave energy converter technology, Proceedings of the Institution of Mechanical Engineers, Part A: Journal of Power and Energy 223 (8) (2009) 887–902.

[4] R. Pelc, R. M. Fujita, Renewable energy from the ocean, Marine Policy 26 (6) (2002) 471–479.

[5] S. P. Beeby, M. J. Tudor, N. M. White, Energy harvesting vibration sources for microsystems applications, Measurement Science and Technology 17 (12) (2006) R175–R195.

[6] Z. L. Wang, New wave power, Nature 542 (7640) (2017) 159–160.

[7] Z. L. Wang, Triboelectric nanogenerators as new energy technology for self-powered systems and as active mechanical and chemical sensors, ACS Nano 7 (11) (2013) 9533–9557.

[8] B. P. Mann, N. D. Sims, Energy harvesting from the nonlinear oscillations of magnetic levitation, Journal of Sound and Vibration 319 (1-2) (2009) 515–530.

[9] B. J. Bowers, D. P. Arnold, Spherical, rolling magnet generators for passive energy harvesting from human motion, Journal of Micromechanics and Microengineering 19 (9) (2009) 094008.

[10] H. Lou, T. Wang, S. Zhu, Design, modeling and experiments of a novel biaxial-pendulum vibration energy harvester, Energy 254 (2022) 124431.

[11] T. Wang, Pendulum-based vibration energy harvesting: mechanisms, transducer integration, and applications, Energy Conversion and Management 276 (2023) 116469.

[12] M. Marszal, B. Witkowski, K. Jankowski, P. Perlikowski, Energy harvesting from pendulum oscillations, International Journal of Non-Linear Mechanics 94 (2017) 251–256.

[13] X. Wang, T. Wang, H. Lv, H. Wang, F. Zeng, Analytical modeling and experimental verification of a multi-dof spherical pendulum electromagnetic energy harvester, Energy 286 (2024) 129428.

[14] Y. Li, Q. Guo, X. Ma, Z. Chen, L. Sun, Study of an electromagnetic ocean wave energy harvester driven by an efficient swing body towards the self-powered ocean buoy application, IEEE Access 7 (2019) 129758–129769.

[15] J. Graves, Y. Kuang, M. Zhu, Scalable pendulum energy harvester for unmanned surface vehicles, Sensors and Actuators A: Physical 318 (2021) 112477.

[16] W. Ding, Z. Mao, H. Cao, K. Wang, Performance evaluation of a two-directional energy harvester with low-frequency vibration, Smart Materials and Structures 29 (5) (2020) 055040.

[17] T. Anurakpandit, N. C. Townsend, P. A. Wilson, The numerical and experimental investigations of a gimballed pendulum energy harvester, International Journal of Non–Linear Mechanics 120 (2020) 103384.

[18] H. Lo, Y.-C. Tai, Parylene-based electret power generators, Journal of Micromechanics and Microengineering 18 (10) (2008) 104006.

[19] Q. Zhang, Y. Wang, E. S. Kim, Electromagnetic energy harvester with flexible coils and magnetic spring for 1–10 hz resonance, Journal of Microelectromechanical Systems 24 (4) (2015) 1193–1206.

[20] P. Maharjan, T. Bhatta, M. S. Rasel, M. Salauddin, M. T. Rahman, J. Y. Park, High-performance cycloid inspired wearable electromagnetic energy harvester for scavenging human motion energy, Applied Energy 256 (2019) 113987.

[21] D. Zhu, S. Beeby, J. Tudor, N. Harris, Increasing output power of electromagnetic vibration energy harvesters using improved Halbach arrays, Sensors and Actuators A: Physical 203 (2013) 11–19.

[22] Y. Jia, Review of nonlinear vibration energy harvesting: Duffing, bistability, parametric, stochastic and others, Journal of Intelligent Material Systems and Structures 31 (7) (2020) 921–944.

[23] T. Haniszewski, J. Margielewicz, D. Gaska, M. Borowiec, M. Bochenski, G. Litak, Y. Kuang, Investigation of energy harvesting efficiency in a magnetic rolling pendulum, Nonlinear Dynamics 113 (2025) 32187–32217.

[24] Y. Li, S. Ma, J. Cao, W. Wang, S. Zhou, An omnidirectional hybrid wind-wave energy harvester based on a coaxial contra-rotation mechanism for unmanned surface vessels, Energy Conversion and Management 289 (2023) 117178.

[25] Liquid Robotics, Wave glider: Over 3 million nautical miles at sea, Web page, accessed 2026-02-04 (2025).
URL `https://www.liquid-robotics.com`

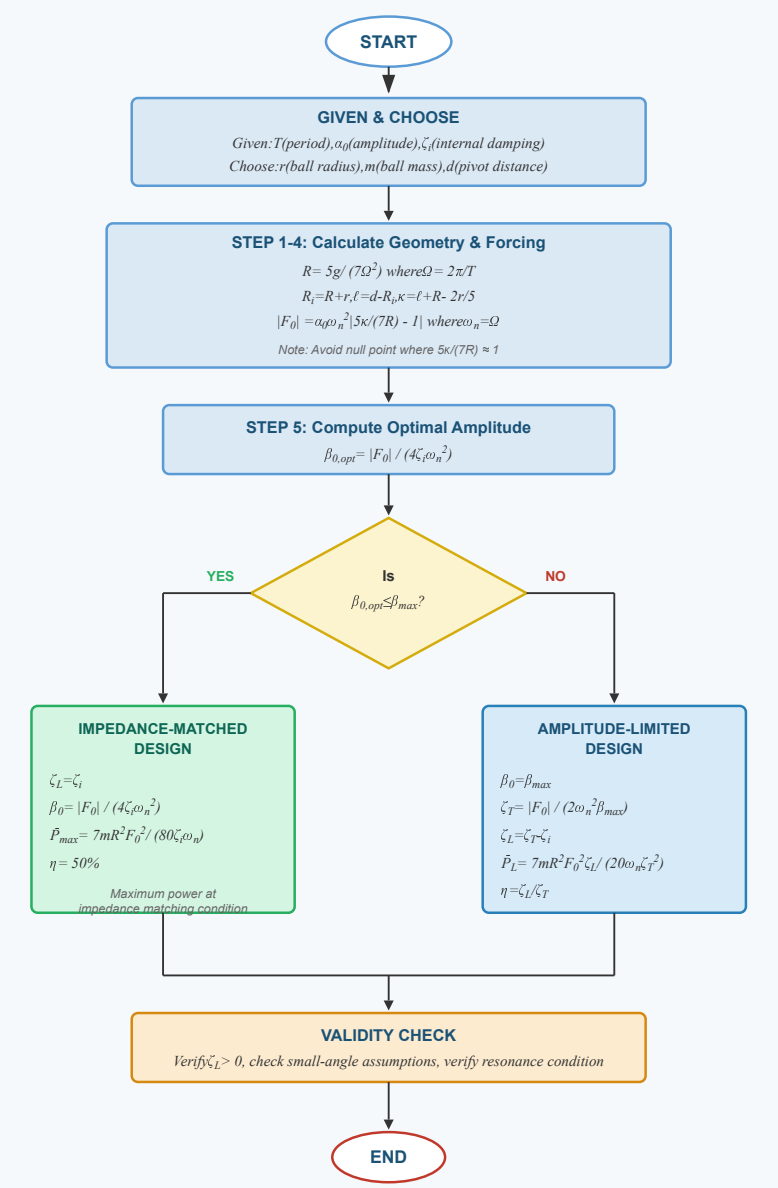

Figure 2: Design flowchart for the ball-in-bowl energy harvester. Given the wave excitation parameters (period T, tilt amplitude α_0) and internal damping ratio ζ_i, the procedure calculates the required bowl radius R for resonance tuning and the normalized forcing amplitude $|F_0|$. The optimal ball oscillation amplitude $\beta_{0,\mathrm{opt}}$ determines whether the system operates in the impedance-matched regime ($\eta = 50\%$) or the amplitude-limited regime where mechanical constraints restrict $\beta_0 \leq \beta_{\max}$.